Journal of Power Sources xxx (2013) 1–6

Contents lists available at SciVerse ScienceDirect

Journal of Power Sources

journal homepage: www.elsevier.com/locate/jpowsour

Diffusion behavior of sodium ions in $Na_{0.44}MnO_2$ in aqueous and non-aqueous electrolytes

Dong Jun Kim [a], Rubha Ponraj [a], Aravindaraj G. Kannan [a], Hyun-Wook Lee [a], Reza Fathi [b], Riccardo Ruffo [b], Claudio M. Mari [b], Do Kyung Kim [a,*]

[a] Department of Materials Science and Engineering, Korea Advanced Institute of Science and Technology (KAIST), 335 Gwahangno, Yuseong-gu, Daejeon 305-701, Republic of Korea
[b] Department of Materials Science, Università degli Studi di Milano-Bicocca, via Cozzi 53, 20125 Milan, Italy

HIGHLIGHTS

- $Na_{0.44}MnO_2$ particles were synthesized by a modified Pechini method.
- Kinetics behavior of sodium ions analyzed in aqueous and non-aqueous electrolytes.
- Better rate capability in aqueous system due to higher apparent diffusion coefficient.
- Also attributed to lower charge transfer resistance and no SEI layer formation.

ARTICLE INFO

Article history:
Received 5 November 2012
Received in revised form
16 January 2013
Accepted 27 February 2013
Available online xxx

Keywords:
Sodium ion battery
Diffusion coefficient
Electrochemical impedance spectroscopy
Sodium manganese oxide
Rate capability

ABSTRACT

The slow kinetics of bigger-sized sodium ions in intercalation compounds restricts the practical applications of sodium batteries. In this work, sodium ion intercalation/de-intercalation behavior of $Na_{0.44}MnO_2$ (NMO), which is one of the promising cathode materials for sodium batteries, is presented in both aqueous and non-aqueous electrolyte systems. The NMO samples synthesized using modified Pechini method shows better rate capability in 0.5 M sodium sulfate aqueous electrolyte system than the 1 M sodium perchlorate non-aqueous system. The difference in the rate performance is extensively investigated using electrochemical impedance spectroscopy (EIS) measurements and the apparent diffusion coefficients of sodium in NMO are determined to be in the range of 1.08×10^{-13} to 9.15×10^{-12} $cm^2\ s^{-1}$ in aqueous system and in the range of 5.75×10^{-16} to 2.14×10^{-14} $cm^2\ s^{-1}$ in non-aqueous systems. The differences in the evaluated rate capability are mainly attributed to nearly two to three orders of magnitude difference in the apparent diffusion coefficient along with the charge transfer resistance and the resistance from the formed SEI layer.

1. Introduction

The application of rechargeable batteries has been growing significantly and has become a key technology in electrochemical energy storage system. Especially, lithium ion (Li-ion) battery has great commercial success in portable electrical devices due to its large energy density and power capabilities compared to other energy storage systems. Recent advances in the renewable energy sources such as solar, wind and biomass have created increasing demands for low-cost and large-scale energy storage systems. Sodium ion (Na-ion) batteries could be a viable option for such large-scale energy storage applications due to the abundant availability of sodium source, similar energy density to Li-ion batteries, potential cost and safety advantages [1–5]. Despite the similarities between sodium and lithium intercalation chemistries, larger Na-ion radius makes it challenging to find suitable sodium intercalating crystal structures.

Recently, various oxides [6–8], phosphates [9,10], fluorophosphates [11] and cyanoferrates [12,13] have been identified as possible candidates for the intercalation of sodium ions. Among the several oxide Na-ion battery materials, $Na_{0.44}MnO_2$ (NMO) is regarded as one of the promising cathode materials owing to its high capacity and good cycle life. Moreover, it can be used in both aqueous and non-aqueous environments. Aqueous electrolyte system has advantages in safety, environmental benignancy and cost issue. Since the pioneering work done by Dahn et al. [14] in aqueous electrolyte battery, there have been successful demonstrations in reversible insertion/desertion of Li/Na in metal oxides

* Corresponding author. Tel.: +82 42 350 4118; fax: +82 42 350 3310.
E-mail address: dkkim@kaist.ac.kr (D.K. Kim).

0378-7753/$ – see front matter © 2013 Elsevier B.V. All rights reserved.
http://dx.doi.org/10.1016/j.jpowsour.2013.02.090

with an aqueous electrolyte condition. Also, NMO can be prepared via facile synthetic methods such as hydrothermal [15,16], solid-state [3], sol–gel [17], polymer-pyrolysis [18] and combustion processes [17]. Although, it exhibits such advantages over other systems, the poor rate capability of NMO in sodium batteries restricts its progress towards practical applications. Sauvage et al. [3] showed that the NMO electrode cycled at C/10 rate displayed a sharp decrease in the capacity, indicating kinetic limitations. Similarly, slow kinetics of the large-sized Na-ions in host matrix is reported for other sodium intercalation compounds [19]. More recently, Cao et al. [18] reported improved rate capability and cyclability using NMO nanowires, which provided shorter diffusion path for sodium insertion/desertion. However, the reported improved rate capability is still much lower in comparison to other lithium-based systems. In addition, the sodium extraction process in NMO involves multi-transition steps during electrochemical reaction as demonstrated in our previous report [20], which indicates complex insertion/desertion processes. Therefore, detailed analysis of the kinetic behavior of sodium ions in NMO materials is needed to exploit this material to commercial success.

In the present work, diffusion behavior of sodium ions in NMO material is studied using cyclic voltammetry and electrochemical impedance spectroscopy. Also, detailed diffusion behavior of sodium ions at each transition voltage is presented. In addition, the diffusion coefficients of sodium in NMO are compared between non-aqueous and aqueous electrolytes and the reason for the discrepancy in diffusion coefficient values are presented.

2. Experimental

2.1. Synthesis and characterization

$Na_{0.44}MnO_2$ particles were synthesized using modified Pechini method, in which, sodium carbonate and manganese acetate were dissolved in distilled water and mixed with citric acid. The resulting transparent solution was heated to evaporate water and form gel. Finally, the gel was calcined at 800 °C for 9 h to remove the organic binders. The prepared material was characterized using scanning electron microscope (SEM) and X-ray diffractometer (XRD).

2.2. Electrochemical test in non-aqueous system

A three-electrode beaker cell was used to evaluate the electrochemical performance of NMO in non-aqueous electrolyte. The working electrode slurry was prepared by mixing synthesized material (75%), conductive carbon black (17%) and PVDF binder (8%) using *N*-methyl-2-pyrrolidone (NMP) solvent. The prepared slurry was coated onto an aluminum foil and dried at 120 °C for 6 h. Metallic sodium and 1 M sodium perchlorate in ethylene carbonate/dimethyl carbonate (EC/DMC − 1:2 v/v) solution were used as anode and electrolyte respectively. Electrochemical measurements were done using Biologic VMP3 multi-channel battery tester at room temperature over the potential range of 3.8–2.0 V vs. Na/Na^+. All the potential values are presented with respect to standard hydrogen electrode (SHE) by subtracting 2.71 V (standard electrode potential for Na/Na^+) to the obtained potential values. All of non-aqueous electrochemical measurements were carried out in argon filled glove box. All the specific capacities mentioned in this article were calculated using the weight of the active materials.

2.3. Electrochemical test in aqueous system

A three-electrode beaker cell was used for the electrochemical characterization in an aqueous system. The electrode composition was same as that of the one used in non-aqueous system except that stainless steel foil was used as current collector. A large size of extracted NMO coated on stainless steel foil and saturated calomel electrodes (SCE) were used as counter and reference electrodes respectively [21]. 0.5 M sodium sulfate solution was used as electrolyte to maintain the same amount of sodium ions as in non-aqueous electrolyte. Galvanostatic charge/discharge cycles were performed in the potential range of 0.65 V to −0.10 V vs. SCE. All the potential values are presented with respect to standard hydrogen electrode (SHE) by adding 0.244 V (standard electrode potential for SCE) to the obtained potential values.

2.4. Diffusion studies

To determine the diffusion coefficients, three-electrode Swagelok cell was used in non-aqueous environment. In this case, slurry of the active material was casted directly on the stainless steel current collector of the cell. Metallic sodium discs were pasted on two different current collectors, and they were used as reference and counter electrodes. The small gap among the electrodes was filled with the electrolyte. Experiments in aqueous electrolyte were performed with the same cell arrangement already described. Cyclic voltammetry (CV) experiments were carried out both in aqueous and non-aqueous environments with the same cell configurations as used in galvanostatic charge/discharge cycling studies. CV was carried out in the potential range of 0–0.65 V vs. SCE in aqueous electrolyte and in the potential range of 2.0–3.8 V vs. Na/Na^+ with the scan rate of 50 $\mu V\ s^{-1}$. The diffusion coefficient of Na-ion in NMO was determined using electrochemical impedance spectroscopy (EIS). The second cycle of CV was interrupted at each peak maximum and EIS was carried out in the frequency range of 100 kHz–3 mHz at the CV interruption voltage with AC amplitude of 10 mV. At each potential, relaxation period of 3 h was allowed prior to EIS measurements.

3. Results and discussion

3.1. Synthesis and characterization

NMO was prepared using modified Pechini method and Fig. 1 shows the XRD pattern of the synthesized NMO. The XRD pattern is indexed to orthorhombic lattice structure (*Pbam* space group), which corresponds to JCPDS card # 27-0750. All Mn^{4+} ions and half of the Mn^{3+} ions are present in the octahedral sites, whereas the

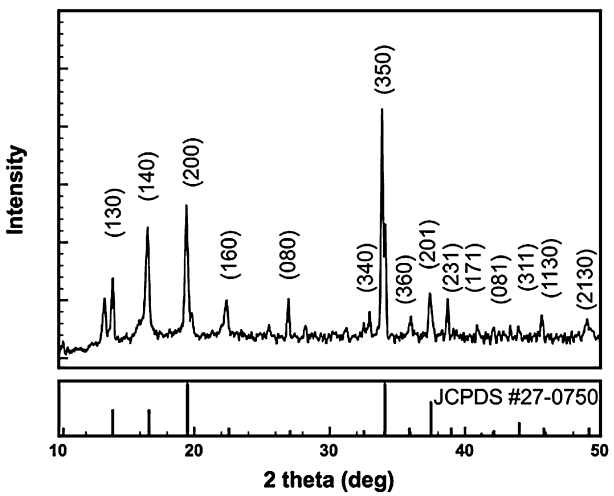

Fig. 1. XRD pattern of the synthesized NMO particles.

Please cite this article in press as: D.J. Kim, et al., Journal of Power Sources (2013), http://dx.doi.org/10.1016/j.jpowsour.2013.02.090

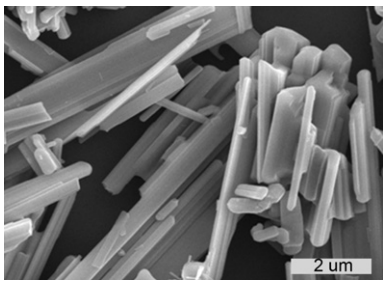

Fig. 2. SEM image of the synthesized NMO particles.

remaining Mn^{3+} ions are present in the square-pyramidal sites. They are arranged to form an S-shaped tunnel, from which sodium ions could be reversibly extracted and a small pentagonal tunnel containing non-extractable sodium ions [22]. The morphology of the synthesized NMO was characterized using SEM and a representative SEM image is shown in Fig. 2. Rod-shaped NMO particles are formed with typical dimensions of a few μm in length and about a 1 μm in width.

3.2. Galvanostatic cycling characteristics

Fig. 3(a) and (b) show the charge–discharge characteristics of NMO in non-aqueous and aqueous electrolytes, respectively at different current rates. The charge–discharge rates (C rate) were calculated based on the theoretical specific capacity of NMO, where 1 C rate corresponds to a current density of 121 mA g^{-1}. The NMO sample in non-aqueous electrolyte exhibits discharge capacities of 65, 59, 47 and 32 mAh g^{-1} at 0.1, 0.2, 0.5 and 1 C rates respectively. This corresponds to specific discharge capacity retention of only 49% when the current rate is increased from 0.1 C to 1 C rate. In general, the discharge curve displays six plateaus at 3.27, 3.22, 3.96, 3.01, 2.55 and 2.15 V (vs. Na/Na^{+}). These plateaus correspond to biphasic transitions, which are attributed to the charge-ordering rather than the long-range sodium ordering.

The discharge curve in aqueous electrolyte shows only three plateaus in the potential range of 0 V–0.65 V (vs. SCE) in comparison with six plateaus in non-aqueous electrolyte system. This can be attributed to the reduction in the potential range in aqueous electrolyte in which NMO electrodes can be cycled. For this reason only part of the sodium ions could be extracted and hence lower specific capacity is expected in aqueous system due to the limited potential window [23]. Another interesting feature in aqueous electrolyte system is its enhanced rate capability. As expected, it shows specific discharge capacity of 40 mAh g^{-1} at 0.1 C rate, which is lower than the specific discharge capacity in non-aqueous electrolyte at the same rate. At higher discharge rates of 0.2 C, 0.5 C and 1 C, NMO displays specific discharge capacities of 39, 36 and 33 mAh g^{-1}, respectively. This corresponds to the capacity retention of 82% when the discharge rate was increased tenfold from 0.1 C to 1 C. It is easy to attribute the difference in the rate capability to the difference in the ionic conductivities of aqueous and non-aqueous electrolytes. In general, lower ionic conductivity in the electrolyte leads to large overpotential (as evidenced in the case of NMO in non-aqueous system) in the charge–discharge curves. Apart from the large overpotential in non-aqueous system, its plateau region also shrinks; whereas the discharge curve of NMO in aqueous electrolyte displays three distinct potential plateaus even at the rate of 1 C. The shortening of the plateau region in the non-aqueous system suggests that the decreased rate capability does not solely arise from the difference in the electrolyte conductivity, but from other electrode processes. In order to determine the cause of such discrepancy between non-aqueous and aqueous systems in the rate capability, diffusion studies were carried out.

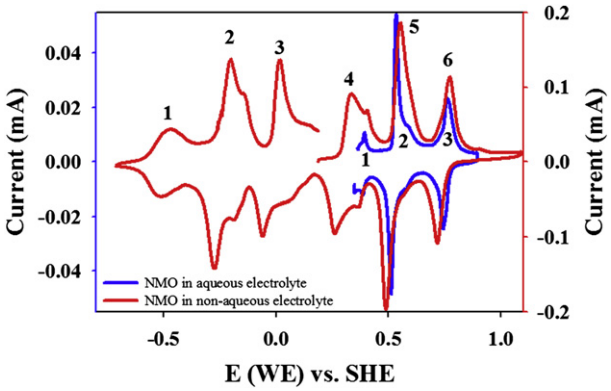

Fig. 4. CV curves of NMO electrode in non-aqueous and aqueous electrolytes.

3.3. Diffusion studies

The CV curves of NMO electrodes in aqueous and non-aqueous electrolytes are shown in Fig. 4. CV curve in non-aqueous electrolyte shows a minimum of six redox processes, which is consistent with the charge–discharge curves. Also, similar results have been published in previous literatures. These processes could be attributed to the extraction of sodium ions from different sites. In case of aqueous electrolyte, only three transition peaks are observed within the studied potential range. Also, the voltage difference

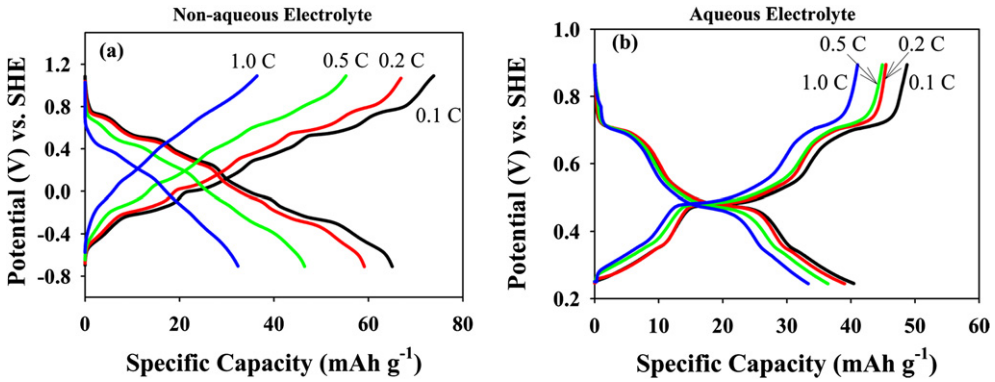

Fig. 3. Rate capabilities of NMO samples in (a) non-aqueous and (b) aqueous electrolytes.

Please cite this article in press as: D.J. Kim, et al., Journal of Power Sources (2013), http://dx.doi.org/10.1016/j.jpowsour.2013.02.090

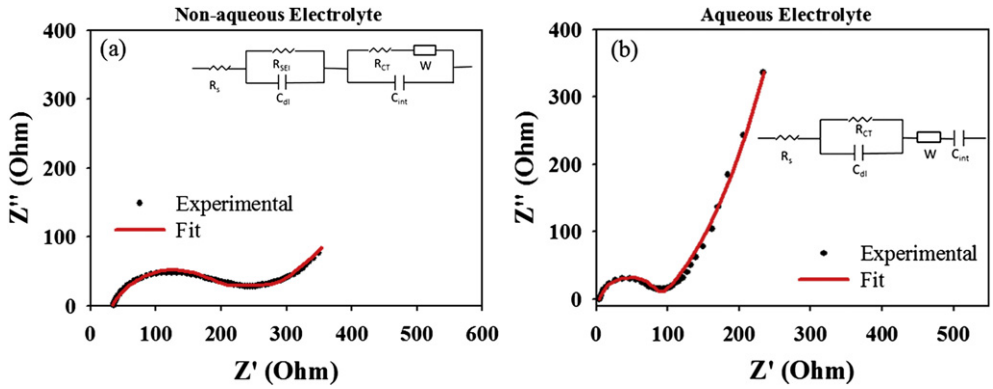

Fig. 5. Representative Nyquist plots of NMO samples measured in (a) non-aqueous and (b) aqueous electrolytes along with their corresponding equivalent circuits given as insets.

between the anodic and cathodic current peaks is much higher in non-aqueous system than in aqueous system. As mentioned earlier, this corresponds to the lower ionic conductivity in the non-aqueous electrolyte in comparison to aqueous electrolyte. CV was interrupted at each transition peak and allowed to equilibrate prior to EIS measurements for determining the diffusion coefficients. Representative Nyquist plots along with the fit are shown in Fig. 5. The sodium ion diffusion coefficients (D_{Na^+}) within NMO in both aqueous and non-aqueous electrolytes were determined from the following equation [24–26] and are presented in Tables 1 and 2, respectively.

$$D_{Na^+} = 0.5\left[\frac{V_m}{nFAZ_w}\left(\frac{dE}{dx}\right)\right]^2 \quad (1)$$

where V_m is the molar volume of NMO (22.85 $cm^3\ mol^{-1}$), F is the Faradaic constant (96,486 C mol^{-1}), A is the contact area between electrode and electrolyte (2.45 $m^2\ g^{-1}$ as determined using BET method), Z_w is Warburg coefficient determined from EIS data, dE/dx is the slope of electrode potential vs. composition determined from galvanostatic discharge curve.

The diffusion coefficient was calculated based on the assumption that the whole surface area of the active material is wetted by the electrolyte in spite of the presence of binder and carbon additive materials. Also, molar volume of the active material is assumed to be constant throughout the intercalation/extraction process despite the changes in the Na-ion composition within the active material during these processes. Hence, the diffusion coefficient values presented in this work are apparent values. As shown in Fig. 6(a), the D_{Na^+} values of sodium within NMO in non-aqueous electrolyte change with the voltage in which the D_{Na^+} value decreases initially as the discharging progressed and starts increasing again on further discharge and vice versa during charging. Similar pattern is observed in the aqueous electrolyte system as well as shown in Fig. 6(b). This behavior can be attributed to the lattice shrinkage/expansion during extraction and intercalation processes, respectively along with the electrostatic repulsion from the sodium ion present within the lattice structures [27]. The diffusion coefficient values of sodium within NMO in aqueous electrolyte range from 1.08×10^{-13} to 9.15×10^{-12} $cm^2\ s^{-1}$; whereas the diffusion coefficient values of sodium within NMO in non-aqueous electrolyte range from 5.75×10^{-16} to 2.14×10^{-14} $cm^2\ s^{-1}$. In general, diffusion coefficient values of sodium ions within NMO in aqueous electrolyte are two to three orders of magnitude higher than the diffusion coefficient values of sodium within NMO in non-aqueous electrolyte. It is well known that the diffusion behavior of ions in the bulk of a material depends on the intrinsic properties of the material and remains same irrespective of the change in the electrolyte. Recently, He et al. [28] demonstrated that the charge transfer resistance in the interface also contributes to the difference in lithium diffusion coefficient values in lithium iron phosphate.

In order to determine the reasons for the variation in the diffusion coefficient values between NMO samples in aqueous and non-aqueous electrolytes, EIS measurements were carried out using three-electrode set-up and the obtained Nyquist plots in non-aqueous and aqueous systems are shown in Fig. 5(a) and (b), respectively and their corresponding equivalent circuits are given as insets. The Nyquist plot of NMO in non-aqueous electrolyte shows two depressed semi-circles in the high and medium frequency region corresponding to Na^+ migration within the SEI layer (R_{SEI}) and charge transfer resistance (R_{ct}), respectively. At low frequency region, the spectra contain a straight line with a slope of approximately 45° corresponding to Warburg diffusion (W) of sodium ions in the bulk. A steeper line is present at very low frequency region indicating the onset of finite length diffusion. In this

Table 1
Diffusion coefficient values during charge and discharge in aqueous electrolyte system.

E (WE) vs. SHE (V)	Diffusion coefficient D_{Na^+}, $cm^2\ s^{-1}$
0.395	7.87E−13
0.531	1.74E−12
0.759	3.68E−13
0.891	9.15E−12
0.738	1.89E−12
0.507	1.08E−13
0.379	2.95E−13
0.341	2.21E−13

Table 2
Diffusion coefficient values in non-aqueous electrolyte at different potentials.

E (WE) vs. SHE (V)	Diffusion coefficient D_{Na^+}, $cm^2\ s^{-1}$
−0.431	2.14E−14
−0.131	5.75E−16
0.046	4.54E−15
0.381	8.53E−15
0.629	2.84E−15
0.832	2.12E−15
1.090	2.24E−15
0.686	5.30E−15
0.444	3.87E−15
0.244	7.71E−16
−0.089	9.59E−16
−0.318	6.27E−15
−0.530	2.04E−14
−0.710	1.82E−15

Please cite this article in press as: D.J. Kim, et al., Journal of Power Sources (2013), http://dx.doi.org/10.1016/j.jpowsour.2013.02.090

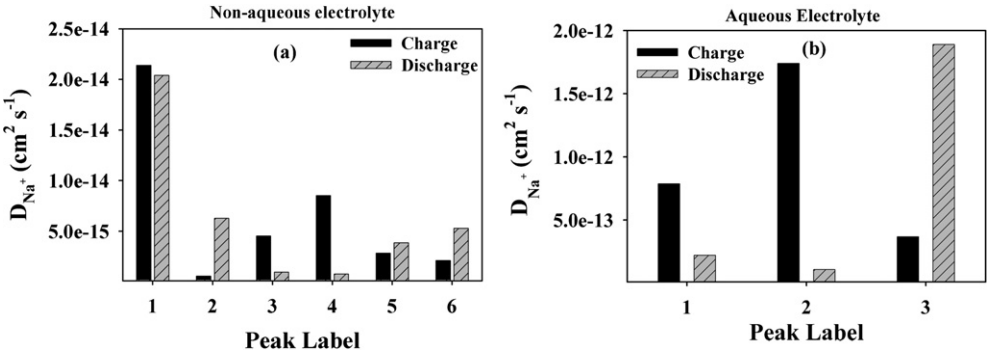

Fig. 6. Diffusion coefficient values of Na^+ ion at the peak positions in (a) 0.5 M Na_2SO_4 solution and (b) 1 M $NaClO_4$ solution.

Table 3
Fitted values of the elements of equivalent circuits used to fit Nyquist plots shown in Fig. 5.

Electrolyte	R_s/Ω	C_{dl}/μF	R_{SEI}/Ω	R_{CT}/Ω	C_{int}/F
Aqueous	2.84	64.15	–	101.20	2.51E−01
Non-aqueous	33.27	37.33	144.10	132.00	2.88E−03

work, constant phase element was used instead of a pure capacitor to account for the presence of depressed semi-circle. Here, C_{dl} corresponds to the SEI layer capacitance and C_{int} is the pseudo-capacitance related to the high surface area as well as the adsorption phenomena at SEI film−NMO electrode surface. In general, the sodium intercalation into NMO is a multi-step process, in which, sodium ions have to first migrate through surface film formed on the electrode followed by insertion into the electrode accompanied by charge transfer resistance and diffusion through the bulk [29,30].

The Nyquist plot obtained in aqueous electrolyte shows a depressed semi-circle in the high−medium frequency range, which corresponds to the charge transfer resistance at the interface and Warburg diffusion at the low frequency region. It should be noted that the fitting of Nyquist plots obtained in aqueous electrolyte requires no additional resistance to account for the formation of SEI layer on the surface. It is well known that SEI layer is formed on the electrode surface during cycling in organic electrolyte to protect active material from further reaction with the electrolyte. The fitted values for each circuit element are given in Table 3. As expected, the solution and Ohmic resistance (R_s) is higher in non-aqueous system than the aqueous system, which could be attributed to the slower ionic conductivity in the non-aqueous electrolyte system. Also, R_{ct} in non-aqueous system is higher than the aqueous system, even though the ionic concentration is maintained same. This could be attributed to the difficulty in desolvation step in non-aqueous electrolyte than the aqueous electrolyte, which may play a key role in blocking the diffusion of ions [28]. In addition, the SEI layer formed on the surface of the electrode resists the migration/diffusion [31] of sodium ions to the bulk of the material and changes the surface concentration of Na-ions at the NMO/SEI/electrolyte interface. Since the diffusion depends on the concentration gradient [32], the apparent diffusion coefficient is also influenced by the nature of the interface itself. So, the apparent diffusion coefficient value measured experimentally in this work is affected by the different interfacial behaviors in aqueous and non-aqueous environments [31,32]. Hence, the discrepancy in the ionic diffusion and rate performance of NMO in aqueous and non-aqueous electrolytes can be attributed to various parameters such as the difficulty in desolvation process and the influence of SEI layer on the interfacial properties.

4. Conclusions

In this work, we analyzed the kinetic behavior of sodium ions in NMO material in non-aqueous and aqueous conditions. NMO showed much better rate capability in aqueous electrolyte condition compared to that of non-aqueous condition. The apparent diffusion coefficient of Na-ion in aqueous condition was in the range of 1.08×10^{-13} to 9.15×10^{-12} cm^2 s^{-1}and 5.75×10^{-16} to 2.14×10^{-14} cm^2 s^{-1} in non-aqueous systems. The differences in the evaluated rate capability were mainly attributed to nearly two to three orders of magnitude difference in apparent diffusion coefficient along with the charge transfer resistance and the additional resistance from the formed SEI layer. Based on these results, we postulate that by improving the charge transfer resistance through surface modification as well as with effective desolvation process on the electrode surface, the rate capability of electrode materials could be enhanced.

Acknowledgements

This work was supported by the Program to Solve Climate Changes (NRF-2010-C1AAA001-2010-0029031), Priority Research Center Program (2011-0031407) and Pioneer Research Center Program (2010-0019469) through the National Research Foundation of Korea (NRF) funded by the Ministry of Education, Science and Technology (MEST). H-W. Lee was financially supported by Basic Science Research Program through the National Research Foundation of Korea (NRF) funded by the Ministry of Education, Science and Technology (2012038593).

References

[1] S.P. Ong, V.L. Chevrier, G. Hautier, A. Jain, C. Moore, S. Kim, X. Ma, G. Ceder, Energy Environ. Sci. 4 (2011) 3680−3688.
[2] V. Palomares, P. Serras, I. Villaluenga, K.B. Hueso, J. Carretero-Gonzalez, T. Rojo, Energy Environ. Sci. 5 (2012) 5884−5901.
[3] F. Sauvage, L. Laffont, J.M. Tarascon, E. Baudrin, Inorg. Chem. 46 (2007) 3289−3294.
[4] N. Yabuuchi, M. Kajiyama, J. Iwatate, H. Nishikawa, S. Hitomi, R. Okuyama, R. Usui, Y. Yamada, S. Komaba, Nat. Mater. 11 (2012) 512−517.
[5] R.A. Huggins, Advanced Batteries: Materials Science Aspects, Springer, New York, 2009.
[6] Z. Lu, J.R. Dahn, J. Electrochem. Soc. 148 (2001) A1225−A1229.
[7] A.D. Tevar, J.F. Whitacre, J. Electrochem. Soc. 157 (2010) A870−A875.
[8] J.F. Whitacre, A. Tevar, S. Sharma, Electrochem. Commun. 12 (2010) 463−466.
[9] P. Moreau, D. Guyomard, J. Gaubicher, F. Boucher, Chem. Mater. 22 (2010) 4126−4128.
[10] L.S. Plashnitsa, E. Kobayashi, Y. Noguchi, S. Okada, J.-I. Yamaki, J. Electrochem. Soc. 157 (2010) A536−A543.
[11] N. Recham, J.N. Chotard, L. Dupont, K. Djellab, M. Armand, J.M. Tarascon, J. Electrochem. Soc. 156 (2009) A993−A999.
[12] C.D. Wessells, R.A. Huggins, Y. Cui, Nat. Commun. 2 (2011) 550.
[13] C.D. Wessells, S.V. Peddada, R.A. Huggins, Y. Cui, Nano Lett. 11 (2011) 5421−5425.
[14] W. Li, J.R. Dahn, D.S. Wainwright, Science 264 (1994) 1115−1118.
[15] Y. Li, Y. Wu, Nano Res. 2 (2009) 54−60.

[16] E. Hosono, H. Matsuda, I. Honma, S. Fujihara, M. Ichihara, H. Zhou, J. Power Sources 182 (2008) 349–352.
[17] M.M. Doeff, T.J. Richardson, J. Hollingsworth, C.-W. Yuan, M. Gonzales, J. Power Sources 112 (2002) 294–297.
[18] Y. Cao, L. Xiao, W. Wang, D. Choi, Z. Nie, J. Yu, L.V. Saraf, Z. Yang, J. Liu, Adv. Mater. 23 (2011) 3155–3160.
[19] S.I. Park, I. Gocheva, S. Okada, J.-I. Yamaki, J. Electrochem. Soc. 158 (2011) A1067–A1070.
[20] H. Kim, D.J. Kim, D.-H. Seo, M.S. Yeom, K. Kang, D.K. Kim, Y. Jung, Chem. Mater. 24 (2012) 1205–1211.
[21] R. Ruffo, C. Wessells, R.A. Huggins, Y. Cui, Electrochem. Commun. 11 (2009) 247–249.
[22] I. Kruk, P. Zajdel, W. van Beek, I. Bakaimi, A. Lappas, C. Stock, M.A. Green, J. Am. Chem. Soc. 133 (2011) 13950–13956.
[23] C. Wessells, R. Ruffomicron, R.A. Huggins, Y. Cui, Electrochem. Solid-State Lett. 13 (2010) A59–A61.
[24] O. Yamada, M. Ishikawa, M. Morita, Electrochim. Acta 45 (2000) 2197–2201.
[25] K.M. Shaju, G.V. Subba Rao, B.V.R. Chowdari, Electrochim. Acta 48 (2003) 2691–2703.
[26] C. Ho, I.D. Raistrick, R.A. Huggins, J. Electrochem. Soc. 127 (1980) 343–350.
[27] J. Xie, K. Kohno, T. Matsumura, N. Imanishi, A. Hirano, Y. Takeda, O. Yamamoto, Electrochim. Acta 54 (2008) 376–381.
[28] P. He, X. Zhang, Y.G. Wang, L. Cheng, Y.Y. Xia, J. Electrochem. Soc. 155 (2008) A144–A150.
[29] G.J. Wang, Q.T. Qu, B. Wang, Y. Shi, S. Tian, Y.P. Wu, R. Holze, J. Power Sources 189 (2009) 503–506.
[30] D. Aurbach, B. Markovsky, I. Weissman, E. Levi, Y. Ein-Eli, Electrochim. Acta 45 (1999) 67–86.
[31] R.N. Methekar, P.W.C. Northrop, K. Chen, R.D. Braatz, V.R. Subramanian, J. Electrochem. Soc. 158 (2011) A363–A370.
[32] C.J. Wen, C. Ho, B.A. Boukamp, I.D. Raistrick, W. Weppner, R.A. Huggins, Int. Met. Rev. 26 (1981) 253–268.

Please cite this article in press as: D.J. Kim, et al., Journal of Power Sources (2013), http://dx.doi.org/10.1016/j.jpowsour.2013.02.090